J. Fluid Mech. (1997), *vol.* 340, *pp.* 297–317. Printed in the United Kingdom

Snakes and corkscrews in core–annular down-flow of two fluids

By YURIKO Y. RENARDY

Department of Mathematics and Interdisciplinary Center for Applied Mathematics, Virginia Polytechnic Institute and State University, Blacksburg, VA 24061-0123, USA

(Received 20 May 1996 and in revised form 21 January 1997)

Core–annular flow of two fluids is examined at the onset of a non-axisymmetric instability. This is a pattern selection problem: the bifurcating solutions are travelling waves and standing waves. The former travel in the azimuthal direction as well as the axial direction and would be observed as corkscrew waves. The standing waves travel in the axial direction but not in the azimuthal direction and appear as snakes. Weakly nonlinear interactions are studied to see whether one of these waves will be stable to small-amplitude perturbations. Sample situations for down-flow are discussed. The corkscrews tend to be preferred when the annulus is narrow, while snakes are more likely when the annulus is wide.

1. Introduction

In perfect core–annular flow of two fluids, the core fluid has a cylindrical interface of uniform radius centred on the pipe axis, surrounded by an annulus of the outer fluid. The response of the flow to perturbations of the form $\exp(in\theta + i\alpha x + \sigma t)$, where θ denotes the azimuthal angle, x the vertical axis, t the time, is examined. When perfect core–annular flow loses stability at a finite axial wavenumber α, with other wavenumbers stable, to an axisymmetric $n = 0$ disturbance, then the interface can deform to a varicose shape (Preziosi, Chen & Joseph 1989; Joseph & Renardy 1993). On the other hand, when the system loses stability to the $n = \pm 1$ non-axisymmetric modes, the critical modes are proportional to $\exp(i\theta + i\alpha x + i\omega t)$, $\exp(-i\theta + i\alpha x + i\omega t)$, and their complex conjugates. Their mode interaction can give rise to either waves travelling in the azimuthal direction (corkscrew waves) or standing waves (snake waves). Both of these waves travel in the axial direction. The snake waves are simply translated along. The corkscrew waves on the other hand travel in both the axial and azimuthal directions (figure 1).

Finite-amplitude corkscrew waves have been observed in the core–annular flow of viscous crude oil and water (see photos in Joseph & Renardy 1993, Chap. VII; and Joseph *et al.* 1997). The experiments of Bai, Chen & Joseph (1992) were conducted in a vertical inverted loop. The oil in the vertical flow experiment is lighter than water so that buoyancy and the pressure gradient act in the same sense in up-flow, where the core oil is observed to produce bamboo waves, and in the opposite sense in down-flow, where the core is compressed and may buckle in corkscrew waves. Sketches of these structures which can be identified with different flow regimes are shown in the review article of Joseph *et al.* (1997). It is possible for the snake mode to be set up initially if the initial condition favours it, for instance when there are bamboo waves in the up-flow part of the loop so that at the top of the loop there is

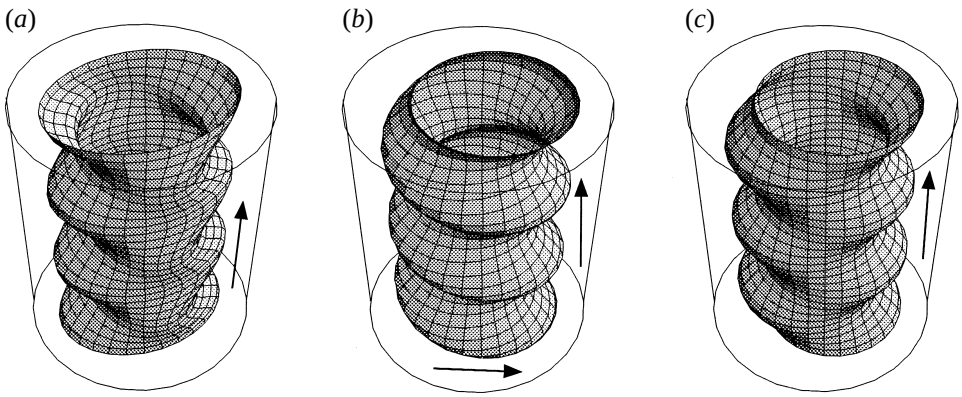

FIGURE 1. (*a*) The $n = 0$ axisymmetric mode. The $n = \pm 1$ non-axisymmetric onset can give rise to (*b*) corkscrews or (*c*) snake waves.

an azimuthal symmetry that favours the solution to be a standing wave. However, if the corkscrews are stable and the snakes not, then this flow would later evolve into the corkscrews.

In this paper, we address the question of whether corkscrew or snake waves bifurcate from perfect core–annular flows. This is a standard Hopf bifurcation with O(2) symmetry, i.e. the problem is invariant under reflection and translation in the azimuthal coordinate θ. In this case, it is known from Ruelle (1973) that if both standing and travelling wave solutions are supercritical, then one of them is stable, and that if one is subcritical, then both are unstable. The equations governing the problem and the weakly nonlinear analysis are detailed in Appendices A and B. Section 4 outlines the application of a centre manifold reduction scheme to the governing equations to derive the weakly nonlinear amplitude evolution equations for the interaction of the two critical Hopf modes. This yields two coupled Landau equations. We note however that for conditions slightly above criticality, an interval of wavenumbers becomes unstable; consequently, there will be development of the disturbances in space as well as in time, and a Ginzburg–Landau equation is usually used. However, the usual Ginzburg–Landau equation does not apply to this problem due to the presence of a long-wave mode for which the decay rate tends to zero in the limit of infinite wavelength. In the context of two-layer plane channel flow, instead of the Ginzburg–Landau equation, a coupled set of equations for three amplitude factors is derived in Renardy & Renardy (1993). The first corresponds to an amplitude of a travelling wave, the second to a long-wave modulation of the interface height, and the third results from the pressure. For core–annular flow, we would have four amplitude factors, two for the azimuthal travelling waves. We have chosen for simplicity to begin with the Stuart–Landau framework. Throughout the analysis, the pressure gradient in the flow direction is assumed to be fixed. An alternative approach would be to keep the flow rate fixed. However, the work of Renardy (1989) on channel flow indicates that there would not be a significant difference with either formulation unless the Reynolds number is high.

In § 4, the stability criteria for the solutions are deduced. In § 5, the pattern selection analysis is carried out for sample conditions in down-flow in which the annular fluid is the more dense. In the first example, the annular fluid is the less viscous, and the preferred pattern is found to be the corkscrews for narrow annuli and snakes for wide

annuli. In the sample case with equal viscosity and free fall, there is a preference for corkscrews, unless the annulus is very wide, in which case snakes are preferred.

2. Formulation of equations

Two immiscible liquids are flowing through a vertical pipe of radius R_2. The governing equations are the Navier–Stokes equations with incompressibility for each fluid. At the interface, the velocity and shear stresses are continuous, the jump in the normal stress is balanced by the effect of interfacial tension, and the kinematic free surface condition holds. The interface between the two liquids is given by $r^* = R(\theta, x, t)$ where (r^*, θ, x^*) denotes cylindrical coordinates, x^* points in the same direction as the centreline base velocity (we non-dimensionalize the flow so that the dimensionless centreline velocity is 1). For upward flow, gravity is acting in the negative x^*-direction, and for downward flow, it is acting in the positive x^*-direction. The flow is driven by a pressure gradient $\mathrm{d}P^*/\mathrm{d}x^* = -f^*$. Asterisks denote dimensional quantities. The pipe axis is at $r^* = 0$. The average value of R is denoted by R_1. The core region $0 \leqslant r^* \leqslant R(\theta, x, t)$ is occupied by fluid 1 with viscosity μ_1 and density ρ_1. Fluid 2, with viscosity μ_2 and density ρ_2, is located in the annulus $R(\theta, x, t) \leqslant r \leqslant R_2$. The following are four dimensionless parameters:

$$m = \mu_2/\mu_1, \quad a = R_2/R_1, \qquad \zeta = \rho_2/\rho_1, \quad K = (f^* + \rho_1 g)/(f^* + \rho_2 g), \tag{2.1}$$

where K measures the ratio of driving forces in the core and annulus.

The dimensionless variables are $(r, x) = (r^*, x^*)/R_1$, $(u, v, w) = (u^*, v^*, w^*)/W_0^*(0)$, $t = t^* W_0^*(0)/R_1$, $p = p^*/[\rho_1 W_0^{*2}(0)]$, where the centreline velocity is

$$W_0^*(0) = (\rho_2 g + f^*)\frac{R_1^2}{4\mu_2}A, \quad A = mK + a^2 - 1 + 2(K-1)\log a. \tag{2.2}$$

The dimensionless base velocity field is $(0, 0, W(r))$ where

$$W(r) = \begin{cases} [a^2 - r^2 - 2(K-1)\log(r/a)]/A, & 1 \leqslant r \leqslant a \text{ (annulus)} \\ 1 - mr^2 K/A, & r < 1 \text{ (core).} \end{cases} \tag{2.3}$$

The base pressure field satisfies

$$\mathrm{d}P/\mathrm{d}x = -f, \quad [\![P]\!] = J/\mathbb{R}_1^2. \tag{2.4}$$

The interfacial tension parameter is

$$J = T^* R_1 \rho_1/\mu_1^2, \tag{2.5}$$

where T^* denotes interfacial tension. This parameter is related to a surface tension parameter introduced by Chandrasekhar (1961) in his study of capillary instability of jets of viscous liquid in air. The Reynolds numbers $\mathbb{R}_i$ are defined by $\mathbb{R}_i = \rho_i W_0^*(0) R_1/\mu_i, i = 1, 2$, where $\mathbb{R}_1/\mathbb{R}_2 = m/\zeta$.

We now perturb perfect core–annular flow so that the total solution is $(u, v, W + w), P + p,\ R/R_1 = 1 + \delta(\theta, x, t)$ and consider the equations for (u, v, w, p, δ). We denote the set of unknowns $(u_1, v_1, w_1, p_1, u_2, v_2, w_2, p_2, \delta)$ by Φ. The governing equations to cubic order are written in the schematic form

$$\mathrm{L}\Phi = \mathrm{N}_2(\Phi, \Phi) + \mathrm{N}_3(\Phi, \Phi, \Phi). \tag{2.6}$$

This is not the amplitude equation but represents the raw governing equations shown in Appendix A. Here the operator L incorporates the linear terms in the differential

equations and bounday conditions, while N_2 stands for the quadratic terms, and N_3 the cubics. The cubic terms arise from the Taylor expansions of the interface conditions. As evident in Appendix A, the continuity equation has been multiplied through by r and the momentum equations by r^2. For small amplitudes, both the quadratic and cubic terms contribute to the cubic nonlinearity in the amplitude equations to be derived in §4. We can write the real linear operator L in the form $A + B\,d/dt$. We also introduce the notation $L(\sigma) = A + \sigma B$. The problem is characterized by six dimensionless parameters: m, a, ζ, J, K and $\mathbb{R}_1$.

3. Linear stability analysis

Non-axisymmetric waves in core–annular flow are mentioned in the linear stability analyses of Preziosi *et al.* (1989) and Boomkamp & Miesen (1992). Hu & Patankar (1995) have performed a linear stability analysis and found parameter regimes for unstable situations, where mode 1 has larger growth rates than mode 0, and correlated the wavelength of maximum growth rate with the observed wavelength for corkscrew waves in the experiments of Bai *et al.* (1992). In their regimes, there are bands of unstable wavelengths for modes 0 and or 1. For example, their figure 2 shows the $n = 1$ mode to be unstable over wavenumbers less than approximately 2, and the $n = 0$ mode unstable for long waves and for wavenumbers approximately between 0.5 and 2.5, while the maximum growth rate is achieved by the $n = 1$ mode at wavenumber approximately 0.5. In this section, we show that there are critical situations where mode 1 onsets at a finite wavelength while other modes are stable. This complements the correlation with the experiments in that the $n = 1$ mode is actually shown to be the first mode to become unstable as a bifurcation parameter is increased.

We replace $[u, v, w, p](r, \theta, x, t)$ and $\delta(\theta, x, t)$ with amplitude functions $[u, v, w, p](r)$ and an amplitude constant δ times $\exp[in\theta + i\alpha x + \sigma t]$ in the usual way. The linearized problem is of the form $(A + \sigma B)\Phi = 0$ where the operators A and B are defined in Appendix A. The Chebyshev-tau scheme (Orszag 1971) is used to discretize this system in the radial direction. To use this, we map each of the regions occupied by the two fluids into $[-1, 1]$. In region i (=1 for the core, 2 for the annulus), $r \to r_i$ where $r_1 = 2r - 1$, $r_2 = 2(r - a)/(a - 1) + 1$. We expand $(u, v, w, p)(r)$ in terms of Chebyshev polynomials $T_k(r_i) = \cos(k \arccos r_i)$. For example,

$$u_1(r) = \sum_{k=0}^{N_1} u_{1k} T_k(r_1), \quad u_2(r) = \sum_{k=0}^{N_2} u_{2k} T_k(r_2). \tag{3.1}$$

We express the derivatives of variables such as u_i and products such as $r_i u_i$ as expansions in Chebyshev polynomials with coefficients that depend on the coefficients u_{ik}. Formulas for these are in Orszag (1971) and Gottlieb & Orszag (1977). In the incompressibility condition, v and w need to be expanded to the same degree polynomial as u' so the expansions for v and w are truncated at the $(N_i - 1)$th Chebyshev polynomial. In the radial component of the equation of motion, p' is required to the same accuracy as u'' so p is also truncated at the $(N_i - 1)$th polynomial. Together with δ, the total is $4N_1 + 4N_2 + 3$ unknowns. In the core, we express the continuity equation, the radial component of the momentum equation and the other two components of the momentum equation, respectively, to degree N_1, $(N_1 - 1)$ and $(N_1 - 2)$, while in the annulus, the momentum equations are expanded to one degree lower. There are seven interface conditions and three boundary conditions to complete the system of equations.

To form the discretized matrices for the operator A, we treat the terms that involve the base flow, e.g. $W(r)r^2u_x$ in fluid i, with a collocation scheme. In the linearized problem, the radial dependence of this term is of the form $f(r_i)u(r_i)$ in fluid i. We use $N+1$ collocation points $r_i = \cos\phi_k$, $\phi_k = k\pi/N$, $k = 0, \ldots, N$ so that $T_n(r_i) = \cos(n \arccos r_i)$ or $T_n(\cos\phi) = \cos n\phi$. At the collocation points, $f(r_i) = f(\cos\phi_k)$ and a Fourier cosine series of this function, extended as an even function over to $-\pi$ so that it is periodic with period 2π gives $f(\cos\phi) = \sum_0^\infty a_n \cos(n\phi)$, which is the Chebyshev series expansion $f(r_i) = \sum_0^\infty a_n T_n(r_i)$. At the collocation points, $f(r_{ik}) = \sum_0^N a_n \cos(n\phi_k) = \sum_0^N C_{kn}a_n$, where C_{kn} is a matrix of collocation values $\cos(n\phi_k)$. The coefficients d_m in $f(r_i)\ u(r_i) = f(\cos\phi_k)\ u(\cos\phi_k) = \sum_{m=0}^N d_m T_m(\cos\phi_k) = \sum_{m=0}^N f(\cos\phi_k)C_{km}u_{im}$ are obtained in terms of the unknowns u_{ik} in (3.1) by noting that $d_n = \sum_{m,k} C_{nk}^{-1} \cos\phi_k C_{km}u_{im}$. Convergence tests were done to decide on the optimal values for the truncations. The numerical results were checked against those of Hu & Patankar (1995) which include the effects of all the parameters, and Joseph, Renardy & Renardy (1983) which treats the case of zero surface tension and equal densities. Our code is independent of the latter code. To compare with these results, we set the density ratio $\zeta = \rho_2/\rho_1$ to one, and $J = 0$; the Reynolds number of Joseph *et al.* (1983) is Re and their complex wave speed is designated as C, related to our $\mathbb{R}_1$ and σ by $Re = a^3\mathbb{R}_1/[(a^2+m-1)m]$, $C = [(a^2+m-1)/a^2](\mathrm{i}\sigma/\alpha)$, where $m = \mu_2/\mu_1 < 1$. The m used by Joseph *et al.* (1983) is μ_1/μ_2. Asymptotic formulas for long and short waves are contained in § VI.1 (h) and § VI.1(i), respectively, of Joseph & Renardy (1993).

4. Analysis of bifurcated solutions for the Hopf–Hopf interaction

Bifurcation from the base solution (2.3)–(2.4) will be investigated for the situation where criticality is achieved at an isolated value of the parameters by a complex eigenvalue $\mathrm{i}\omega$ at axial wavenumber α and azimuthal wavenumber $n = 1$ and another eigenvalue $\mathrm{i}\omega$ at the same α but azimuthal wavenumber $n = -1$.

In the x- and θ-directions, the solution is assumed to be periodic and expanded in a Fourier series. The operator $\mathrm{L}(\sigma)$ has a one-dimensional nullspace at the zeroth Fourier mode ($\mathrm{d}/\mathrm{d}x = 0$, $\mathrm{d}/\mathrm{d}\theta = 0$) with $p =$ constant and the other variables equal to zero due to the fact that we can add an arbitrary constant to the pressure. To make the pressure unique we normalize it.

We reduce the partial differential equations and boundary conditions governing the problem (given in Appendix A) to two complex-valued ordinary differential equations by applying the centre manifold reduction scheme. The reduction to the centre manifold is described in Renardy (1989) for the two-layer Couette–Poiseuille flow, and the methodology is analogous here. In the following, we shall take the existence of a centre manifold for granted and do formal calculations. We view one of the fluid parameters, e.g. the Reynolds number, as a bifurcation parameter. For instance, we set $\lambda = Re - Re_c$, where Re_c is the critical value of a Reynolds number. Close to criticality ($\lambda = 0$) we denote by $\omega_1(\lambda)$ the eigenvalue which arises from perturbing $\mathrm{i}\omega$, by $\zeta_1(\lambda)$ the eigenfunction belonging to $\omega_1(\lambda)$ at azimuthal wavenumber $n = 1$, and by $\zeta_2(\lambda)$ the eigenfunction belonging to $n = -1$, satisfying

$$\mathrm{L}(\omega_1(\lambda))\zeta_k(\lambda) = 0, \quad k = 1, 2. \tag{4.1}$$

The eigenfunction ζ_2 is retrieved from ζ_1 by the azimuthal reflection $n \to -n$, $v \to -v$. The eigenfunction computed in § 3 is used for $\zeta_1(0)$. The two eigenfunctions

have the forms

$$\zeta_1 = \tilde{\zeta}_1(r)\exp(\mathrm{i}\alpha x + \mathrm{i}\theta), \quad \zeta_2 = \tilde{\zeta}_2(r)\exp(\mathrm{i}\alpha x - \mathrm{i}\theta). \tag{4.2}$$

The inner product $(\cdot,\cdot)$ at the discretized level corresponds to a weighted L_2 inner product, in which the components of the first function are complex conjugated. At the continuum level, this is $(g_1, g_2) = \int_{-1}^{1} \bar{g}_1(\tilde{r})g_2(\tilde{r})(1-\tilde{r}^2)^{-1/2}\mathrm{d}\tilde{r}$. The Chebyshev expansions of g_1, g_2 in $\tilde{r}$ results in a double summation under the integral sign, which is calculated with the use of the orthonormalization condition $\int_{-1}^{1} T_n(\tilde{r})T_m(\tilde{r})(1-\tilde{r}^2)^{-1/2}\mathrm{d}\tilde{r} = (\pi/2)c_n\delta_{nm}$, $c_0 = 2$, $c_n = 1$ for $n > 0$. We drop the factors $c_n\pi/2$ and define a discretized inner product of two functions g_1 and g_2, expanded in Chebyshev polynomials, $g_1 = \sum_{i=0}^{N} g_{1i}T_i(\tilde{r})\exp(\mathrm{i}\alpha_1 x + \mathrm{i}\xi_1\theta)$, $g_2 = \sum_{i=0}^{N} g_{2i}T_i(\tilde{r})\exp(\mathrm{i}\alpha_2 x + \mathrm{i}\xi_2\theta)$, $\tilde{r} = r_1$ or r_2, to be

$$(g_1, g_2) = \frac{\displaystyle\int_0^{2\pi} \exp[\mathrm{i}(-\xi_1+\xi_2)\theta]\ \mathrm{d}\theta \int_0^{C} \exp[\mathrm{i}(-\alpha_1+\alpha_2)x]\ \mathrm{d}x}{\displaystyle\int_0^{2\pi}\mathrm{d}\theta\int_0^{C}\mathrm{d}x} \sum_{i=0}^{N} \bar{g}_{1i}g_{2i}.$$

Here, C represents a period in x, that is a multiple of $2\pi/\alpha$. Thus, unless $-\alpha_1+\alpha_2 = 0$ and $-\xi_1+\xi_2 = 0$, the inner product vanishes because of periodicity.

The eigenfunction b_1 to the adjoint problem satisfies $(b_1, \mathrm{L}(\omega_1(\lambda))\Phi) = 0$, where Φ is arbitrary, and has the same dependence on θ and x as the respective eigenfunctions ζ_1. The adjoint eigenvector corresponding to ζ_1 has the form $b_1 = \tilde{b}_1(r)\exp(\mathrm{i}\alpha x + \mathrm{i}\theta)$. In our calculations, we do not need to calculate the eigenfunction to the adjoint problem, because we shall discretize the linear operator and perform the inner products involving the adjoint problem based on finite-dimensional matrices. If $\boldsymbol{L}_d$ is the matrix representing the discretized form of the operator L, then the discretized b_k is the eigenvector of the adjoint matrix $\bar{\boldsymbol{L}}_d^T$ with eigenvalue $\bar{\omega}_1$. In weakly nonlinear theory, the solution is expanded as $\Phi \sim \sum_{i=1}^{2} z_i\zeta_i + \sum_{i=1}^{2}\bar{z}_i\bar{\zeta}_i + \ldots$, where z_i are complex time-dependent amplitude functions. Appendix B contains the derivation of the amplitude equations:

$$\left.\begin{aligned} \mathrm{d}z_1/\mathrm{d}t &= \omega_1(\lambda)z_1 + \beta_1(\lambda)|z_1|^2 z_1 + \beta_2(\lambda)|z_2|^2 z_1, \\ \mathrm{d}z_2/\mathrm{d}t &= \omega_1(\lambda)z_2 + \beta_1(\lambda)|z_2|^2 z_2 + \beta_2(\lambda)|z_1|^2 z_2, \end{aligned}\right\} \tag{4.3}$$

$\omega_1(\lambda) = \mathrm{i}\omega + \epsilon_1$, where ω and the bifurcation parameter ϵ_1 are real. The coefficients β_i obtained through the projections are defined in Appendix B. The equilibrium solutions are given in the following.

4.1. *Travelling waves (corkscrews)*

For the travelling waves, one of the z_i is zero. The corkscrews travel in the azimuthal as well as the axial directions. We denote $z_1 = r_1\exp(\mathrm{i}r_2 t)$, where

$$r_1^2 = -\epsilon_1/\mathrm{Re}\ (\beta_1,) \quad r_2 = \omega + \mathrm{Im}\ (\beta_1)r_1^2, \quad z_2 = 0. \tag{4.4}$$

The solution is supercritical if $-\epsilon_1/\mathrm{Re}\ (\beta_1) > 0$, and since the base flow is stable for $\epsilon_1 < 0$, we require $\mathrm{Re}\ (\beta_1) < 0$ for the solution to exist above threshold. If this condition is satisfied, then the solution branch is said to be 'supercritical'. Since our bifurcation problem involves a two-fold degeneracy, supercriticality alone is not enough to imply the stability of that solution branch to small perturbations, and there will be a further condition to be satisfied.

Once we have a solution $(z_1, z_2) = (a, 0)$, we can generate a family of solutions $(a\exp(\mathrm{i}\phi), 0)$ by a shift in the axial or azimuthal directions or in time. To examine the stability of this solution, we set $z_1 = (r_1 + \tilde{z}_1)\exp(\mathrm{i}r_2 t), z_2 = \tilde{z}_2\exp(\mathrm{i}r_2 t)$. In the transformed system, we introduce perturbations $\tilde{z}_1 = y_1\exp(\Lambda t)$, $\tilde{z}_2 = y_2\exp(\Lambda t)$, $\bar{\tilde{z}}_1 = y_3\exp(\Lambda t)$, and $\bar{\tilde{z}}_2 = y_4\exp(\Lambda t)$. The eigenvalues determining stability are $\Lambda = (-\beta_1 + \beta_2)r_1^2$ and its complex conjugate, 0, and $-2\epsilon_1$. Thus for stability we require

$$\mathrm{Re}\ (\beta_1) < 0, \text{ and } \mathrm{Re}\ (\beta_2) < \mathrm{Re}\ (\beta_1). \tag{4.5}$$

The zero eigenvalue is due to the one-parameter family of solutions which is generated by a shift in t or θ. The appearance of the zero eigenvalue can be interpreted alternatively in terms of the dimension of the torus covered by the solution (Fujimura & Renardy 1995). The travelling wave solution represents a periodic orbit or a 1-torus. The one-parameter family of solutions generated by the phase shifts simply moves the original solution along the trajectory curve, and therefore the solution covers, in total, a 1-torus.

4.2. *Standing waves (snakes)*

The snake waves have both amplitudes $|z_1| = |z_2|$ non-zero. We denote $z_1 = r_1\exp(\mathrm{i}r_2 t)$ where

$$r_1^2 = -\epsilon_1/(\mathrm{Re}\ (\beta_1) + \mathrm{Re}\ (\beta_2)), \quad r_2 = \omega + (\mathrm{Im}\ (\beta_1) + \mathrm{Im}\ (\beta_2))r_1^2. \tag{4.6}$$

This solution exists for $\epsilon_1 > 0$ if $(\mathrm{Re}\ (\beta_1) + \mathrm{Re}\ (\beta_2)) < 0$, and this is the condition for the snake solution to be a supercritical branch. In order to get an autonomous system for the stability analysis, we transform out the factor $\exp(\mathrm{i}r_2 t)$ by substituting $z_1 = (\tilde{z}_1 + r_1)\exp(\mathrm{i}r_2 t), z_2 = (\tilde{z}_2 + r_1)\exp(\mathrm{i}r_2 t)$. Linearizing about the base solution, we again introduce perturbations $\tilde{z}_1 = y_1\exp(\Lambda t)$, and so on. The standing wave solution is symmetric in the sense that the reflection $\theta \to -\theta, v \to -v, z_1 \to z_2$ leaves the solution the same. Therefore the perturbations can be decoupled into even modes $(z_1 = z_2, \bar{z}_1 = \bar{z}_2)$ and odd modes $(z_1 = -z_2, \bar{z}_1 = -\bar{z}_2)$. The eigenvalues are $0, 0, -2\epsilon_1, 2(\mathrm{Re}(\beta_1) - \mathrm{Re}(\beta_2))r_1^2$. There are two zero eigenvalues, related to the fact that the standing wave solution covers a 2-torus. The solution (4.6) is a 1-torus, and the shift in θ generates a one-parameter family covering a 2-torus. The shift in x or t simply moves the solution along its trajetory and does not generate a new manifold of solutions. For stability, we require the two conditions

$$\mathrm{Re}\ (\beta_1 + \beta_2) < 0, \text{ and } \mathrm{Re}\ (\beta_1) < \mathrm{Re}\ (\beta_2). \tag{4.7}$$

5. Pattern selection results

We present results for down-flows. The base velocity profiles for the cases we consider are shown in figure 2(*a–c*). Since core–annular flows can admit base flows that are downward in one region and upward in another, we define down-flows to be those in which gravity is acting in the same direction as the dimensional centreline velocity.

Some of the pattern selection results will be given in tabular form. For the tabulated values of the wavenumbers α, the corresponding $\mathrm{Im}(\sigma)$ are given. The ϵ_1 of the previous section denotes a perturbation to $\mathrm{Re}(\sigma)$ as the bifurcation point is traversed. The calculation of the Landau coefficients yields the preferred pattern.

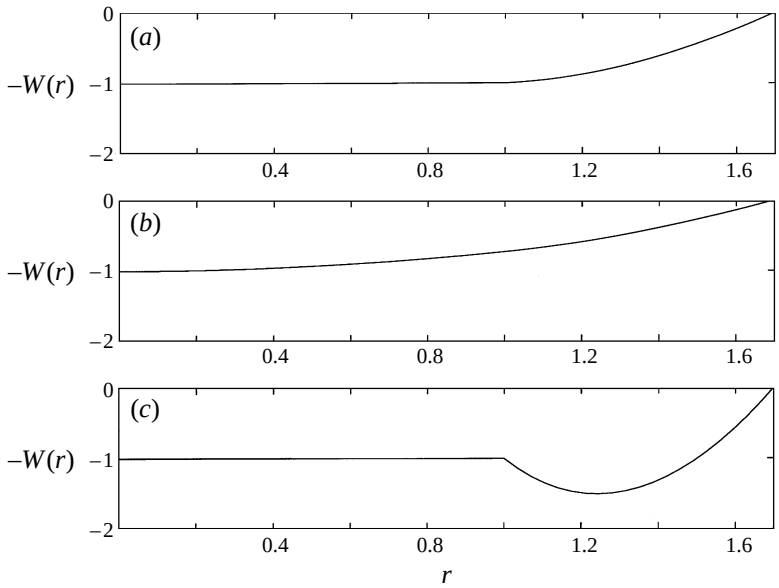

FIGURE 2. Base velocity profiles representing the down-flows discussed in § 5. (*a*) $m = 0.03$, $a = 1.7$, $K = 0.10429$, $\zeta = 1.1$; (*b*) $m = 1$, $\zeta = 2$, $a = 1.7$, $K = 0.5$; (*c*) $m = 0.00166$, $\zeta = 1.1$, $a = 1.7$, $K = -0.5427$.

5.1. *Critical conditions*

We begin with the parameters of Hu & Patankar (1995, figure 3*b*): $a = 1.4$, $m = 0.01$, $\zeta = 1.1$, $\mathbb{R}_1 = 1$, $J = 0$. Here, the $n = 0, 1$ modes are stable for long waves, the $n = 1$ achieves the maximum growth rate at wavenumber $\alpha \approx 1.7$, and the other modes are also unstable. The effect of adding surface tension is the stabilization of the higher modes, shorter waves, and a destabilization of the axisymmetric mode due to capillary instability. We balance these effects and choose $J = 0.01$, for which the axisymmetric mode is only slightly destabilized, while the $n \geqslant 2$ modes are stabilized, leaving only the $n = 0, 1$ modes unstable. By varying the density ratio ζ from 0.8 to 1.1, the magnitudes of the instabilities change but the signs are not affected; we choose $\zeta = 1.1$. There is more sensitivity to the radius ratio a and the viscosity ratio m. When $a = 1.5, 1.6$, mode 1 develops long-wave instability. Mode 1 is further destabilized as a increases as reported by Hu & Patankar (1995). Mode 1 is stable for $a = 1.1, 1.2, 1.3$. Slight increases in m stabilize both modes, namely at $m = 0.02$ the window of instability for mode 0 shrinks while that for mode 1 remains similar. At $m = 0.03$, mode 0 is stable while mode 1 retains a window of instability. At $m = 0.04$, mode 1 develops a long-wave instability as well as a separate window of $O(1)$ wave instability $0.3 \leqslant \alpha \leqslant 1.6$. In the search for a mode 1 criticality, we retain $m = 0.03$ and examine a between 1.3 and 1.4. The delicate dependence on a is shown in figure 3(*a*). In this manner a criticality is found for $a = 1.37, \alpha = 1.3, \sigma = -0.0004 - 1.26\mathrm{i}$ (there is no round-off error in these values; in order to get $\mathrm{Re}(\sigma)$ closer to 0, we need to evaluate the critical values of a and α to more significant figures than we have given. These values for criticalities are sufficiently accurate for the application of the ensuing nonlinear analysis). The growth rates are shown in figure 3(*b*) for modes 0 to 2. Higher modes and shorter waves are effectively stabilized by surface tension. The wavenumbers in the range $1 < \alpha < 1.5$ are all close to criticality. The Reynolds number is slightly increased in figure 3(*c*), resulting in the wavenumbers around 2.5

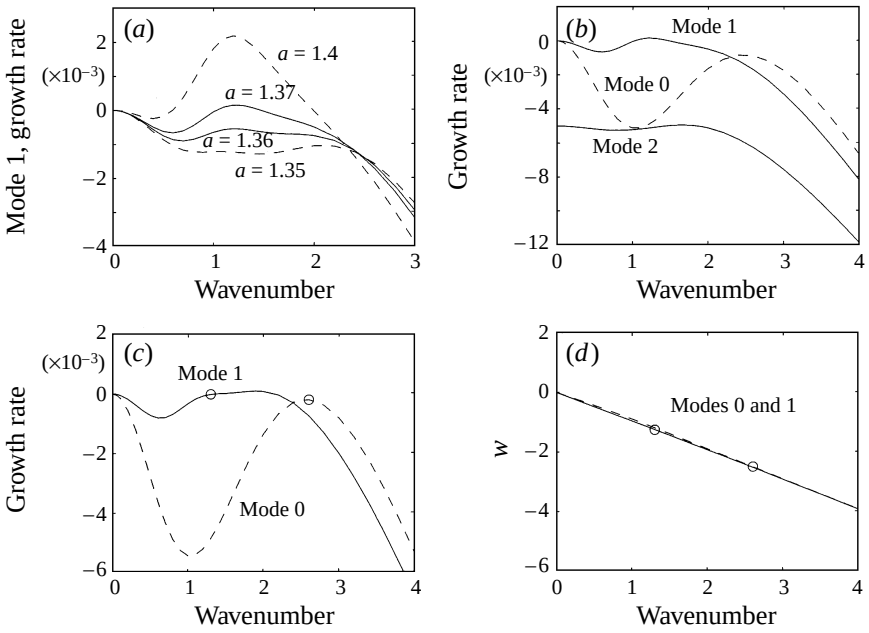

FIGURE 3. (*a*) Growth rate $\mathrm{Re}(\sigma)$ versus wavenumber α for $J = 0.01$, $\mathbb{R}_1 = 1$, $m = 0.03$, $\zeta = 1.1$, mode 1. Effect of varying a. (*b*) Growth rate versus wavenumber for $J = 0.01$, $m = 0.03$, $a = 1.37$, $\mathbb{R}_1 = 1$, $\zeta = 1.1$, $K = 0.10429$. Mode 1 is at criticality. Modes 0,2, and higher are stable. (*c*) Growth rate versus wavenumber for $J = 0.01$, $m = 0.03$, $a = 1.37$, $\mathbb{R}_1 = 1.06$, $\zeta = 1.1$, $K = 0.10429$. Mode 1 at $\alpha = 1.3$ and mode 0 at $\alpha = 2.6$ are resonant and circled. (*d*) For the parameters of (*c*), the imaginary part of the eigenvalue $\mathrm{Im}(\sigma) = w$ is plotted against α. Both modes 0 and 1 coincide, and circles denote the resonant values corresponding to those of (*c*).

for mode 0 coming close to criticality, and the wavenumbers 1 to 2.5 for mode 1 being slightly above onset.

The critical situation of figure 3(*b*) is close to a resonant 2:1 mode interaction, namely, mode 1 is at criticality with wavenumber $\alpha_c = 1.3$ and eigenvalue $\mathrm{i}\omega = -1.26\mathrm{i}$, and mode 0 is critical with wavenumber $2\alpha_c$ and eigenvalue $2\mathrm{i}\omega$. The Reynolds number is increased slightly for figure 3(*c*, *d*) to show that an interval of wavenumbers is close to onset. Figure 3(*c*, *d*) shows the real and imaginary parts of the eigenvalues at these wavenumbers. For the $\alpha = 1.3$, mode 1, onset, for instance, a proper analysis should incorporate the resonant interaction, and would show the existence of new solutions that involve both modes 0 and 1. A diagnostic for the occurrence of resonant situations is that the Landau coefficients become sensitive to small changes. In our case, this is due to a near-singular matrix in the calculation of the interaction term ψ_{12} (see Appendix B), and a pole for the Landau coefficient β_2. Table 1 shows that the Landau coefficient β_1, which determines the supercriticality of the corkscrews, varies smoothly, while the imaginary part of β_2 changes from negative and large at $\alpha = 1.2$ to positive and large at $\alpha = 1.3$, indicating that there is a pole here. The last column denotes the solution type: in addition to the 'c' and 's', stable corkscrews and snakes, both supercritical, we have situations where only one solution is supercritical and therefore both solutions are unstable. Thus, 'cx' in the last column denotes the supercriticality of corkscrews but not snakes. The numerical results indicate that at resonance, there is a change from a situation where snakes are subcritical and corkscrews are supercritical to a situation where both are supercritical and corkscrews

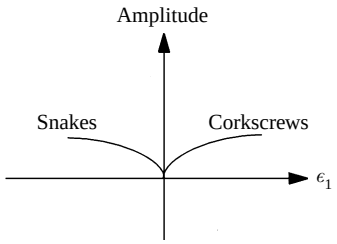

FIGURE 4. Bifurcation diagram close to resonance. $m = 0.03$, $\zeta = 1.1$, $J = 0.01$, $K = 0.10429387$, $a = 1.37$, $\mathbb{R}_1 = 1$, $\alpha = 1.3$, mode 1 onset.

α	Im (σ)	β_1	β_2	Pattern
1.0	−0.97	−12 + 62i	5 − 109i	s
1.1	−1.06	−10 + 59i	7 − 196i	s
1.2	−1.16	−8 + 56i	8 − 629i	cx
1.3	−1.26	−6 + 53i	− 24 + 680i	c
1.4	−1.36	−5 + 50i	− 3 + 242i	s
1.5	−1.45	−3 + 49i	0.5 + 157i	s
1.9	−1.85	−1 + 47i	3 + 87i	cx
2.0	−1.94	−1 + 48i	3 + 83i	cx

TABLE 1. $a = 1.37$, $\mathbb{R}_1 = 1.0$, $m = 0.03$, $\zeta = 1.1$, $K = 0.10429387$, $J = 0.01$. The last column indicates stable snakes (s) or stable corkscrews (c) when both solutions are supercritical; cx denotes the supercritical corkscrews when snakes are subcritical and both solutions are unstable.

are stable. The results in table 1 do not account for the interaction of the $n = 0$ and $n = \pm 1$ modes. When the Reynolds number is increased to $\mathbb{R}_1 = 1.06$, these numerical results are robust. There is sensitivity to changes in a. Figure 4 shows the bifurcation diagram as the parameter ϵ_1 varies.

When a changes from 1.37, the modes shift away from being resonant (figure 5(a) shows $a = 1.45$). Table 2 lists the conditions for which mode 1 is the critical mode and other modes are stable. As the annular gap widens, it is found that the critical mode shifts from 1 to 0. Figure 5(b) shows this for $a = 1.9$: mode 0 is already unstable at $\mathbb{R}_1 = 0.3$ for $0 < \alpha < 0.9$ while other modes are stable. Thus, table 3 lists the conditions for which mode 1 is neutral at onset, while mode 0 is already unstable due to capillary effects. When the Reynolds number $\mathbb{R}_1$ is increased, the added shear has a stabilizing effect on the capillary instability for mode 0 while mode 1 is destabilized. At $a = 1.9$, either mode 0 is unstable for lower Reynolds numbers or both modes 0 and 1 are unstable for higher Reynolds numbers, with mode 1 becoming more unstable than mode 0 (at $a = 1.9$, $\mathbb{R}_1 = 0.4$, mode 0 is unstable for $0.4 < \alpha < 0.9$ with maximum growth rate $\mathrm{Re}(\sigma) = 0.0005$ at $\alpha = 0.7$, mode 1 is unstable for $0 < \alpha < 0.7$ with $\mathrm{Re}(\sigma) = 0.002$ at $\alpha = 0.6$, thus mode 1 has the higher growth rate). In these cases where mode 1 dominates the instability at slightly higher Reynolds numbers, the nonlinear analysis for the neutral situations listed in table 3 may be relevant. In both tables 2 and 3, the last columns denote the solution type: s denotes stable snakes, c denotes stable corkscrews. Both solution types are supercritical for $\epsilon_1 > 0$, the regime where the base flow is unstable, so that one type is stable. The trend is that snakes are preferred when the annular gap is wider.

The base velocity profiles for the situations in tables 2 and 3 are of the type shown in figure 2(a). Note that since the dimensional centreline velocity $W_0^*(0) =$

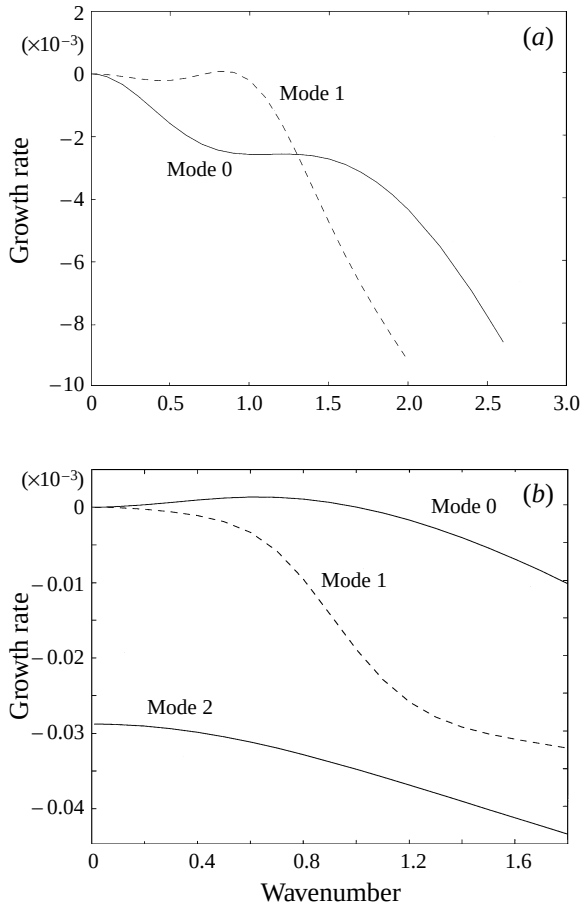

FIGURE 5. Growth rate versus wavenumber for $J = 0.01$, $m = 0.03$, $\zeta = 1.1$, $K = 0.10429$. (*a*) $a = 1.45$, $\mathbb{R}_1 = 0.6$; (*b*) $a = 1.9$, $\mathbb{R}_1 = 0.36$.

a	$\mathbb{R}_1$	α	Im (σ)	β_1	β_2	Pattern
1.37	1.0	1.3	−1.26	−6 + 53i	−25 + 680i	c
1.4	0.8	1.0	−0.98	−27 + 55i	−4 − 65i	s
1.45	0.6	0.8	−0.79	−41 + 17i	−1 − 19i	s
1.5	0.5	0.7	−0.70	−21 + 0.3i	−0.7 − 9i	s
1.6	0.43	0.6	−0.61	−5 − 0.2i	−0.5 − 3i	s
1.7	0.38	0.5	−0.51	−2 + 0.7i	−0.3 − 0.9i	s

TABLE 2. Critical conditions for $m = 0.03$, $\zeta = 1.1$, $K = 0.10429387$, $J = 0.01$. The last column shows whether the snakes or corkscrews are stable.

$(\rho_1-\rho_2)gR_1^2A/[(K-1)4\mu_2]$, the sign of gravity is the same as the sign of $(1-\zeta)A/(K-1)$. Thus, for our parameters, g is positive and points in the same direction as the centreline velocity; this signifies down-flow. For $K = 0.10429$ and $\zeta = 1.1$, we see from $f^*/(\rho_1 g) = (1 - \zeta K)/(K - 1)$ that the applied pressure gradient f^* acts in the opposing sense to gravity and almost balances out the effect of gravity for the core fluid.

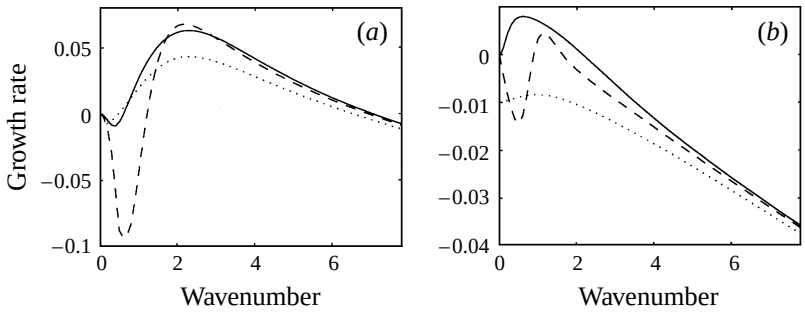

FIGURE 6. Growth rate versus wavenumber for free fall, $\zeta = 1.1$, $K = 1/\zeta$, $m = 0.001$, $\mathbb{R}_1 = 1$, (*a*) $a = 1.2$, (*b*) $a = 1.9$. Modes 0 (solid line), 1 (dashed) 2 (dotted).

a	$\mathbb{R}_1$	α	Im (σ)	β_1	β_2	Pattern
1.8	0.37	0.5	−0.51	$-1 + 0.9$i	$-0.4 - 0.09$i	s
1.9	0.36	0.5	−0.52	$-0.6 + 0.9$i	$-0.5 + 0.2$i	s

TABLE 3. Conditions for mode 1 to be neutral. Mode 0 onsets at a lower Reynolds number. $m = 0.03$, $\zeta = 1.1$, $K = 0.10429387$, $J = 0.01$. The last column shows whether the snakes or corkscrews are stable.

5.2. *Free fall*

In free fall ($f^* = 0$), $K = 1/\zeta$. We begin by considering the same fluid parameters as above ($m = 0.03$, $\zeta = 1.1$, $\mathbb{R}_1 = 1$, $J = 0.01$), and find that mode 0 onsets first. The pattern selection analysis is performed at the wavenumber of maximum growth rate close to neutral situations for mode 1. In table 4(*a*), $m = 0.03$, $\zeta = 1.1$, mode 0 attains the largest growth rate for $a = 1.4$ and mode 1 for $a = 1.5$ (the growth rate profile is similar to figure 6*a*) and higher. At yet larger values of a, for example $a = 5$, only mode 0 is unstable. This is due to capillary effects for the relatively thin filament at the core, since the shear rate at the interface is of small scale. Corkscrews are preferred unless the annulus width becomes large. A decrease in the Reynolds number eventually leads to mode 0 attaining the largest growth rate due to capillary instability. For the Reynolds number in table 4(*b*), for instance, mode 1 has the largest growth rates for $a = 1.6$ and higher, while mode 0 has the largest growth rates for the lower values of a. The growth rates here are however small, and we have applied the pattern selection analysis at the points of maximum growth rates. The results remain robust at the neutral situations, for example the $a = 1.2$ entry in table 4(*b*) becomes neutral with $\alpha = 4.2$ at $\mathbb{R}_1 = 0.7$, where corkscrews are again stable. Calculations were performed for lower Reynolds numbers where mode 1 attains neutral conditions and, for example, at Reynolds number 0.6, the preferred patterns for $a = 1.3$ to 1.6 of table 4(*b*) remain the same. The results in table 4 indicate that when there is more of the annular fluid, snakes are preferred while corkscrews are preferred, when the annulus is narrow. This trend is also observed at other values of m, namely $m = 0.1, 0.001$. At $m = 0.1$, $\mathbb{R}_1 = 1$, mode 0 attains the largest growth rate for $a = 1.3$ to 1.5 while for higher $a = 1.6$ to 1.9, mode 1 attains the largest growth rate. The pattern selection analysis is performed at the largest growth rate wavenumber for mode 1. Again, the corkscrews are stable when the annulus is not too wide, $a = 1.3$ to 1.7, and snakes are stable when $a = 1.8,\ 1.9$. At $m = 0.001$, $\mathbb{R}_1 = 1,\ 1.5$, mode 1 has

	a	α	Im (σ)	β_1	β_2	Pattern
(a) $\mathbb{R}_1 = 1$	1.4	2.8	−2.6	−2.2 + 40i	−2.6 + 38i	c
	1.5	2.2	−2.1	−1.9 + 27i	−2.1 + 25i	c
	1.6	1.8	−1.7	−1.67 + 18i	−1.71 + 15i	c
	1.7	1.6	−1.5	−1.44 + 13i	−1.35 + 10i	s
	1.8	1.4	−1.3	−1.16 + 9i	−1.04 + 7i	s
	1.9	1.3	−1.3	−0.97 + 7i	−0.78 + 5i	s
	2.0	1.2	−1.2	−0.8 + 5i	−0.6 + 3i	s
	3.0	0.8	−0.8	−0.1 + 0.9i	0.03 + 0.5i	s
(b) $\mathbb{R}_1 = 0.8$	1.2	4.6	−4.0	−0.8 + 32i	−1 + 30i	c
	1.3	3.4	−3.1	−1.4 + 40i	−1.8 + 39i	c
	1.4	2.6	−2.4	−1.6 + 34i	−1.8 + 31i	c
	1.5	2.2	−2.1	−1.540 + 27i	−1.538 + 24i	s
	1.6	1.8	−1.7	−1.36 + 18i	−1.25 + 15i	s
	1.7	1.6	−1.5	−1.21 + 13i	−0.97 + 11i	s
	1.8	1.4	−1.3	−1.0 + 9i	−0.8 + 7i	s
	1.9	1.3	−1.3	−0.9 + 7i	−0.6 + 5i	s

TABLE 4. Pattern selection analysis is performed at the maximum growth rate wavenumber for mode 1 at $m = 0.03, \zeta = 1.1, K = 1/\zeta, J = 0.01$, free fall.

a	α	Im (σ)	β_1	β_2	Pattern
1.2	0.4	−0.15	−1.3 − 50i	−1.5 − 90i	c
1.3	0.7	−0.36	−0.8 − 24i	−1.1 − 30i	c
1.4	0.8	−0.49	−0.6 − 13i	−0.9 − 9i	c
1.5	0.8	−0.55	−0.5 − 8i	−0.8 − 3i	c
1.6	0.8	−0.60	−0.4 − 5i	−0.7 − 0.9i	c
1.7	0.8	−0.63	−0.4 − 4i	−0.7 − 0.1i	c
1.8	0.7	−0.58	−0.3 − 2i	−0.5 − 0.1i	c
1.9	0.7	−0.60	−0.3 − 2i	−0.4 − 4i	c
2.0	0.7	−0.61	−0.25 − 1.5i	−0.36 − 0.08i	c
2.1	0.6	−0.54	−0.18 − 0.9i	−0.24 − 0.09i	c
2.3	0.6	−0.55	−0.16 − 0.6i	−0.19 − 0.1i	c
3.0	0.4	−0.39	−0.056 − 0.09i	−0.04 − 0.07i	s

TABLE 5. Pattern selection analysis is performed at the maximum growth rate wavenumber for mode 1 at $m = 1,\ \zeta = 2,\ K = 1/\zeta,\ J = 0.01,\ \mathbb{R}_1 = 1$, free fall.

the larger growth rate for the smaller $a = 1.2$ to 1.6 and mode 0 for the larger $a = 1.7$ to 1.9 (figure 6). It is interesting that in the previous cases, the trend was the reverse. The pattern selection analysis for $\mathbb{R}_1 = 1$ at the largest growth rate wavenumber for mode 1 yields stable corkscrews for $a = 1.2$ to 1.5 and stable snakes for $a = 1.6$ and higher.

Next, consider free fall for equal viscosity and a heavier fluid outside: $m = 1$, $\zeta = 2$, $K = 0.5$, $\mathbb{R}_1 = 1$. The base flow for $a = 1.7$ is shown in figure 2(b). This case is focused on the effect of density stratification. For $a = 1.2$ to 3 in table 5, only mode 1 is unstable. Modes 0 and 2 are stable (see figures 7a, b), and in particular, mode 1 changes smoothly from figure 7(a) to 7(b). At $a = 1.1$, all modes are stable. For the cases $a = 1.2$ to 3, mode 1 is unstable for long waves, and achieves a maximum growth rate at an order-1 wavenumber. The pattern selection results in table 5 favour corkscrews unless the annulus is large. For larger annulus values, such as $a = 5$, mode 1 is stabilized and mode 0 is destabilized by capillarity. Calculations were also

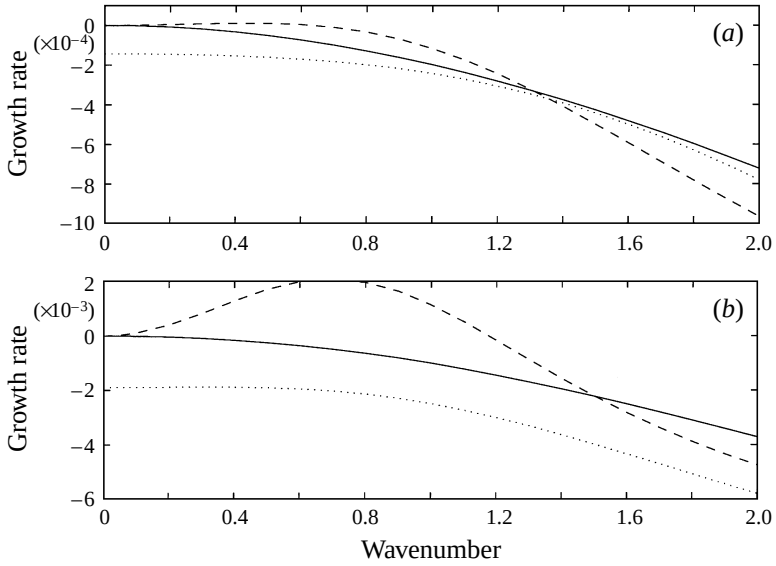

FIGURE 7. Growth rate versus wavenumber for free fall, $\zeta = 2$, $K = 0.5$, $m = 1$, $\mathbb{R}_1 = 1$. (*a*) $a = 1.2$ Line styles as figure 6. (*b*) $a = 1.9$.

performed at the neutral stability points, e.g. $a = 1.9, \alpha = 1.2, \sigma = -0.0001-\mathrm{i}$, and again the preference for corkscrews is robust.

5.3. *Experiments of Bai, Chen & Joseph (1992)*

Figure 3 of Joseph *et al.* (1997) shows a variety of flow types in down-flow in a vertical pipeline experiment with oil and water, which was earlier reported in Bai *et al.* (1992). Flow type (*c*) in the regime called 'disturbed core annular flow' consists of corkscrew waves. There is some variation in the observed data: the conditions may not be exactly steady and the arrangement may have narrower annuli. Snake waves were not observed. Further details are given in Hu & Patankar (1995, §4) where the parameters are $\mathbb{R}_1 = 1.2$, $a = 1.7$, $m = 0.00166$, $\zeta = 1.1$, $K = -0.54270708$; their figure 2 shows that mode 1 has the largest growth rate at $\alpha = 0.531$ and mode 0 has much smaller growth rates, though it has two bands of unstable wavelengths, one for long waves due to interfacial tension and the other at $O(1)$ wavenumbers due to shear. They show that the wavelengths and wave speeds agree with the experimental values. Under these conditions, we need to examine what would happen if only the non-axisymmetric mode were excited. This could occur, for instance, if the initial condition favours it. We can also cover a range of Reynolds numbers while keeping the relative driving forces K constant, to examine neighbouring regimes. When the Reynolds number $\mathbb{R}_1$ is decreased, the $O(1)$ wavenumber instabilities are stabilized since these are primarily due to shear, while the long-wave axisymmetric modes are destabilized due to capillary breakup. Thus, as the Reynolds number is decreased, the growth rates for mode 1 decrease, while those of the longer waves at mode 0 increase and overtake them at approximately $\mathbb{R}_1 = 0.2$. This is illustrated in figure 8. We show the pattern selection results in figure 9 for $0.2 < \mathbb{R}_1 < 1.4$ which includes the parameter values of interest. The base velocity profile is of the type in figure 2(*c*). Figure 10 shows the pattern selection results at another wavenumber $\alpha = 0.4$ where mode 1 attains largest growth rates for the lower Reynolds numbers, showing

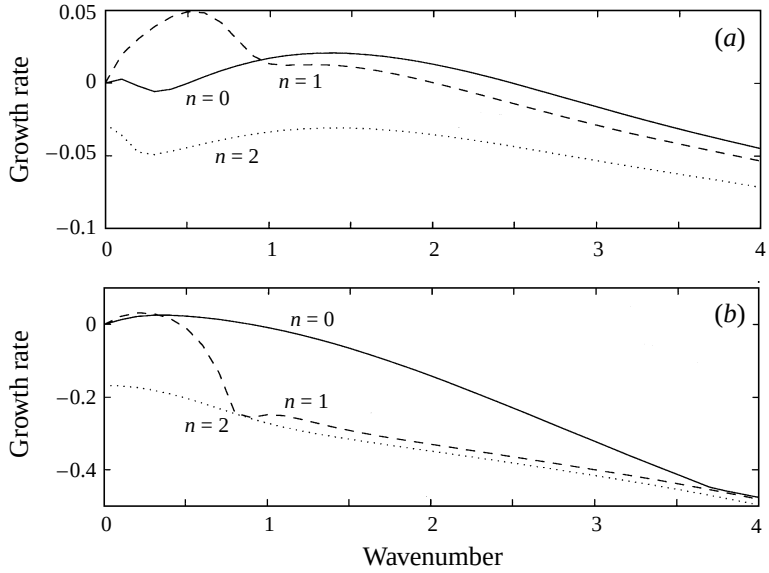

FIGURE 8. Growth rates versus wavenumber for $K = -0.5427$, $a = 1.7$, $\zeta = 1.1$, $m = 0.00166$, $J = 0.06$. (*a*) $\mathbb{R}_1 = 1.2$, (*b*) $\mathbb{R}_1 = 0.2$.

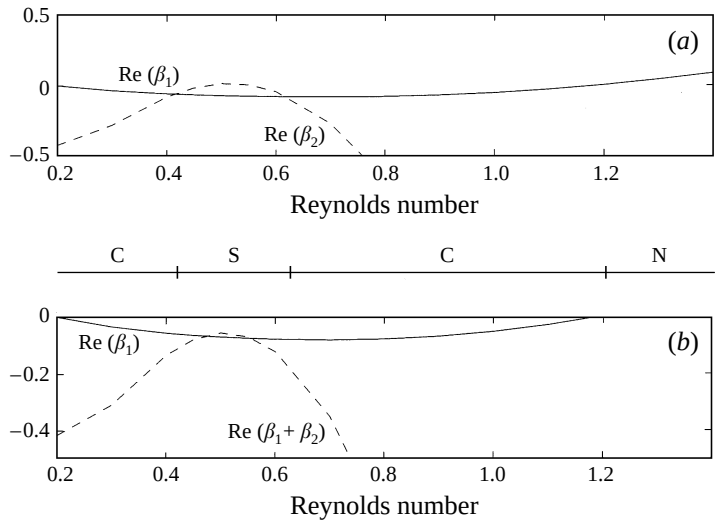

FIGURE 9. Pattern selection results for $K = -0.5427$, $a = 1.7$, $\alpha = 0.531$, $\zeta = 1.1$, $m = 0.00166$, $J = 0.06$. (*a*) The real parts of the Landau coefficients (cf. (4.5), (4.7)); a stability condition for corkscrews is that Re (β_2) < Re (β_1), and vice versa for snakes. (*b*) The second stability condition, that of supercriticality, for corkscrews is that Re (β_1) < 0, and for snakes that Re ($\beta_1 + \beta_2$) < 0. The results from both (*a*) and (*b*) are combined in the middle plot to show the intervals of Reynolds numbers $\mathbb{R}_1$ in which corkscrews (C) are preferred, snakes (S) are preferred, or neither (N).

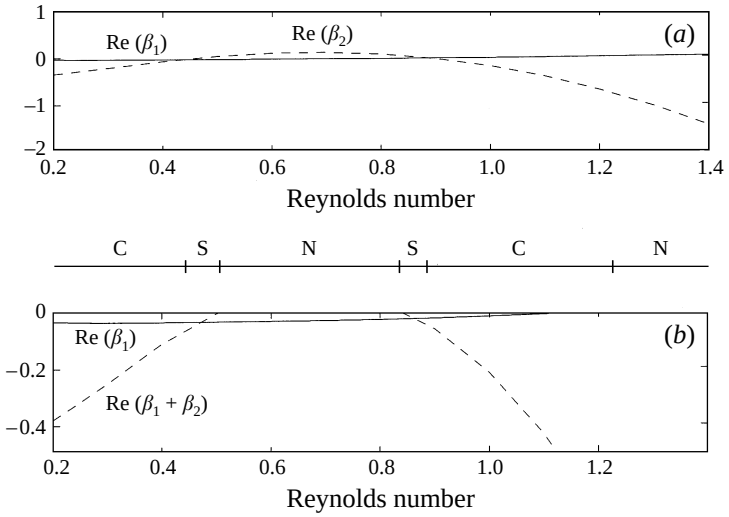

FIGURE 10. As figure 9 but for $\alpha = 0.4$.

the preference for corkscrews around $\mathbb{R}_1 = 1.2$. It is interesting that our bifurcation analysis shows this and that snake waves were not observed in the experiments.

This work was supported by the National Science Foundation under Grant No. CTS-9307238, No. CTS-9612308 and the Office of Naval Research under Grant No. N00014-92-J-1664. Part of this work was performed at the Isaac Newton Institute for Mathematical Sciences and as Visiting Fellow at Clare Hall, Cambridge (UK).

Appendix A. Definition of the operators

The governing equations, interface and boundary conditions are represented schematically in the form $\mathrm{L}\Phi = \mathrm{N}_2(\Phi,\Phi) + \mathrm{N}_3(\Phi,\Phi,\Phi)$, where L, N_2, N_3 are the linear, quadratic and cubic operators, respectively, and Φ is the perturbation to the base flow (2.3)–(2.4). We write $\mathrm{L}\Phi = \mathrm{A}\Phi + (\mathrm{d}/\mathrm{d}t)\mathrm{B}\Phi$. These operators may be represented by eighteen components: incompressibility and three components of the momentum equation in each fluid, three boundary conditions, and seven interface conditions. The corresponding components of $\mathrm{N}_2(\Phi,\Phi)$ are denoted by $(H_1, H_2, \ldots, H_{18})$, and those of $\mathrm{N}_3(\Phi,\Phi,\Phi)$ by $(Q_1, \ldots, Q_{18})$. No nonlinear terms appear in the incompressibility condition and the boundary conditions on the walls, and therefore the corresponding components of N_2 and N_3 are zero. The other components of N_2 are labelled H_1 to H_{18}, and similarly the $Q_i, i = 1, \ldots, 18$, in accordance with the labelling of the components below. The nonlinear terms appear in computations in the form $\mathrm{N}_2(f,g)$ and $\mathrm{N}_3(f,g,h)$. With the following definition for the components of $\mathrm{N}_2(\Phi,\Phi)$, we define $\mathrm{N}_2(f,g)$ to be the average of the two permutations $\mathrm{N}_2(f,g)$ and $\mathrm{N}_2(g,f)$. For example, if $\mathrm{N}_2(\Phi,\Phi) = \Phi\partial\Phi/\partial x$, then $\mathrm{N}_2(f,g) = 0.5(f\partial g/\partial x + g\partial f/\partial x)$. Similarly, $\mathrm{N}_3(f,g,h)$ is defined as one sixth of the six possible permutations of the cubic expression. Primes denote $\partial/\partial r$. $[\![x]\!] = x_1 - x_2$. The normal $\boldsymbol{n}$ and tangents $\boldsymbol{t}_1, \boldsymbol{t}_2$ to the interface are $\boldsymbol{n} = \nabla F/|\nabla F|$, the interface position is $r = R/R_1 = 1 + \delta$, $\nabla F = \boldsymbol{e}_r - (R_\theta/R)\boldsymbol{e}_\theta - R_x\boldsymbol{e}_x$, $\boldsymbol{t}_1 = (\boldsymbol{e}_\theta + (R_\theta/R)\boldsymbol{e}_r)[1 + (R_\theta^2/R^2)]^{-1/2}$, $\boldsymbol{t}_2 = (\boldsymbol{e}_x + R_x\boldsymbol{e}_r)(1 + R_x^2)^{-1/2}$. The normal stress condition is $\boldsymbol{n}\cdot[-([\![P + p]\!]\rho_1 W_0^2 + 2H^*T^*)\boldsymbol{n} + [\![2\mu D[\boldsymbol{u}^*]]\!]\cdot\boldsymbol{n}] = 0$, where T^* is the surface tension coefficient, $D[\boldsymbol{u}^*] = (1/2)(\nabla u^* + \nabla u^{*T})$, $\boldsymbol{u}^*$ is the total dimensional

velocity, $\nabla \boldsymbol{u}^*$ is

$$(W_0^*(0)/R_1)\begin{pmatrix} u_r & v_r & w_r + W_r \\ \frac{1}{r}u_\theta - \frac{v}{r} & \frac{1}{r}v_\theta + \frac{u}{r} & \frac{1}{r}w_\theta \\ u_x & v_x & w_x \end{pmatrix}. \tag{A 1}$$

The curvature is $2H^* = (RR_{\theta\theta}(1 + R_x^2) + RR_{xx}(R^2 + R_\theta^2) - R^2(1 + R_x^2) - 2R_\theta^2 - 2RR_\theta R_x R_{x\theta})/(R^2 + R_\theta^2 + R^2R_x^2)^{3/2}$. The shear stress conditions are $[\![\boldsymbol{t}_i \cdot 2\mu D[\boldsymbol{u}^*] \cdot \boldsymbol{n}]\!] = 0,\ i = 1, 2.$

In the core region $0 \leqslant r \leqslant 1$ (subscript 1),

$$(\mathrm{A}\Phi)_1 = ru' + u + rw_x + v_\theta,$$
$$(\mathrm{A}\Phi)_2 = W(r)r^2u_x + (\rho_1/\rho)r^2p' - (1/\mathbb{R}_i)\Big(- u + ru' + r^2u'' + u_{\theta\theta} + r^2u_{xx} - 2v_\theta\Big),$$
$$(\mathrm{A}\Phi)_3 = W(r)r^2v_x + (\rho_1/\rho)rp_\theta - (1/\mathbb{R}_i)\Big(- v + rv' + r^2v'' + v_{\theta\theta} + r^2v_{xx} + 2u_\theta\Big),$$
$$(\mathrm{A}\Phi)_4 = ur^2W'(r) + w_xr^2W(r) + (\rho_1/\rho)r^2p_x - (1/\mathbb{R}_i)\Big(rw' + r^2w'' + w_{\theta\theta} + r^2w_{xx}\Big).$$

The corresponding expressions for the annulus $1 \leqslant r \leqslant a$ (subscript 2) are denoted $(\mathrm{A}\Phi)_5, \ldots, (\mathrm{A}\Phi)_8$. The interface conditions are the kinematic condition, the continuity of velocity and stress components, and the normal stress condition which are given in full in Joseph & Renardy (1993, chap. II.1, p. 47). Expanded for small perturbations, these are, respectively, at $r = 1$,

$$(\mathrm{A}\Phi)_9 = W_1\delta_x - u(1), \qquad (\mathrm{A}\Phi)_{10} = u_1 - u_2,$$
$$(\mathrm{A}\Phi)_{11} = v_1 - v_2, \qquad (\mathrm{A}\Phi)_{12} = w_1 - w_2 + \delta W_1' - \delta W_2',$$
$$(\mathrm{A}\Phi)_{13} = [\![(\mu/\mu_1)(w' + u_x)]\!] + \delta[\![(\mu/\mu_1)W'']\!], \qquad (\mathrm{A}\Phi)_{14} = [\![(\mu/\mu_1)(v' + u_\theta - v)]\!],$$
$$(\mathrm{A}\Phi)_{15} = -\mathbb{R}_1[\![p]\!] - (J/\mathbb{R}_1)(\delta + \delta_{\theta\theta} + \delta_{xx}) + 2[\![(\mu/\mu_1)u']\!].$$

The boundary conditions yield $(\mathrm{A}\Phi)_{16} = u$, $(\mathrm{A}\Phi)_{17} = v$, and $(\mathrm{A}\Phi)_{18} = w$ at $r = a$. The components of $\mathrm{B}\Phi$ are

$$(\mathrm{B}\Phi)_1 = 0, \quad (\mathrm{B}\Phi)_2 = r^2u_1, \quad (\mathrm{B}\Phi)_3 = r^2v_1, \quad (\mathrm{B}\Phi)_4 = r^2w_1, \quad (\mathrm{B}\Phi)_5 = 0,$$
$$(\mathrm{B}\Phi)_6 = r^2u_2, \quad (\mathrm{B}\Phi)_7 = r^2v_2, \quad (\mathrm{B}\Phi)_8 = r^2w_2, \quad (\mathrm{B}\Phi)_9 = \delta,$$

and $(\mathrm{B}\Phi)_i = 0, i = 10, \ldots, 18$. The quadratic components in fluid 1 are

$$H_1 = 0, \qquad H_2 = -r^2uu' - rvu_\theta + rv^2 - r^2wu_x,$$
$$H_3 = -r^2uv' - rvv_\theta - ruv - r^2wv_x, \qquad H_4 = -r^2uw' - rvw_\theta - r^2ww_x,$$

and the corresponding components in fluid 2 are $H_5, \ldots, H_8$. The interface conditions at $r = 1$ contribute

$$H_9 = -\delta\delta_xW_1' + \delta u_1' - w_1\delta_x - v_1\delta_\theta, \qquad H_{10} = -\delta u_1' + \delta u_2',$$
$$H_{11} = -\delta v_1' + \delta v_2', \qquad H_{12} = -\delta w_1' + \delta w_2' - \tfrac{1}{2}\delta^2W_1'' + \tfrac{1}{2}\delta^2W_2'',$$
$$H_{13} = -\delta[\![(\mu/\mu_1)(w'' + u_x')]\!] - \delta_x[\![(2\mu/\mu_1)(u' - w_x)]\!] + \delta_\theta[\![(\mu/\mu_1)(w_\theta + v_x)]\!]$$
$$-\tfrac{1}{2}\delta^2[\![(\mu/\mu_1)W''']\!],$$
$$H_{14} = -\delta[\![(\mu/\mu_1)(v'' + u_\theta' - v' - u_\theta + v)]\!] - 2\delta_\theta[\![(\mu/\mu_1)(u' - v_\theta - u)]\!]$$
$$+\delta_x[\![(\mu/\mu_1)(w_\theta + v_x)]\!],$$
$$H_{15} = \mathbb{R}_1\delta[\![p']\!] - 2\delta[\![(\mu/\mu_1)u'']\!] + (J/\mathbb{R}_1)\Big(\tfrac{1}{2}(-\delta_\theta^2 + \delta_x^2) - \delta^2 - 2\delta\delta_{\theta\theta}\Big)$$
$$+2\delta\delta_x[\![(\mu/\mu_1)W'']\!] + 2\delta_\theta[\![(\mu/\mu_1)(u_\theta + v' - v)]\!] + 2\delta_x[\![(\mu/\mu_1)(u_x + w')]\!],$$

$H_i = 0, i = 16, \ldots, 18$. The only contributions to cubic terms come from the interface conditions. $Q_i = 0, i = 1, \ldots, 8, 16, \ldots, 18$. At $r = 1$,

$$Q_9 = -\tfrac{1}{2}\delta^2\delta_x W_1'' + \tfrac{1}{2}\delta^2 u_1'' - \delta w_1'\delta_x + v_1\delta\delta_\theta - \delta v_1'\delta_\theta,$$
$$Q_{10} = -\tfrac{1}{2}\delta^2 u_1'' + \tfrac{1}{2}\delta^2 u_2'', \qquad Q_{11} = -\tfrac{1}{2}\delta^2 v_1'' + \tfrac{1}{2}\delta^2 v_2'',$$
$$Q_{12} = -\tfrac{1}{2}\delta^2 w_1'' + \tfrac{1}{2}\delta^2 w_2'' - \tfrac{1}{6}\delta^3 W_1''' + \tfrac{1}{6}\delta^3 W_2''',$$

$$Q_{13} = -\tfrac{1}{2}\delta^2[\![(\mu/\mu_1)(w''' + u_x'')]\!] - \delta\delta_x[\![(2\mu/\mu_1)(u'' - w_x')]\!] + \delta_\theta\delta_x[\![(\mu/\mu_1)(v' + u_\theta - v)]\!]$$
$$+\delta\delta_\theta[\![(\mu/\mu_1)(w_\theta' + v_x' - v_x - 2w_\theta)]\!]$$
$$+\delta_x^2[\![(\mu/\mu_1)(w' + u_x)]\!] + \delta_x^2\delta[\![(\mu/\mu_1)W'']\!] - \tfrac{1}{6}\delta^3[\![(\mu/\mu_1)W^{iv}]\!],$$
$$Q_{14} = -\delta^2[\![(\mu/\mu_1)\Big(\tfrac{1}{2}(v''' + u_\theta'' - v'') - u_\theta' + v' + u_\theta - v\Big)]\!] + \delta_\theta^2[\![(\mu/\mu_1)(v' + u_\theta - v)]\!]$$
$$-2\delta\delta_\theta[\![(\mu/\mu_1)(u'' - v_\theta' - 2u' + 2v_\theta + 2u)]\!] + \delta_x\delta_\theta[\![(\mu/\mu_1)(w' + u_x)]\!]$$
$$+\delta\delta_x\delta_\theta[\![(\mu/\mu_1)W'']\!] + \delta_x\delta[\![(\mu/\mu_1)(w_\theta' + v_x' - w_\theta)]\!],$$
$$Q_{15} = \mathbb{R}_1\tfrac{1}{2}\delta^2[\![p'']\!] - (J/\mathbb{R}_1)\Big(\tfrac{1}{2}\delta\delta_x^2 - \tfrac{3}{2}\delta\delta_\theta^2 + \tfrac{3}{2}\delta_{\theta\theta}\delta_\theta^2 + \tfrac{1}{2}\delta_{\theta\theta}\delta_x^2 + \tfrac{1}{2}\delta_{xx}\delta_\theta^2 + \tfrac{3}{2}\delta_{xx}\delta_x^2$$
$$-\delta^3 + 2\delta_\theta\delta_x\delta_{\theta x} - 3\delta^2\delta_{\theta\theta}\Big) - \delta^2[\![(\mu/\mu_1)u'']\!] + \delta^2\delta_x[\![(\mu/\mu_1)W''']\!]$$
$$+4\delta\delta_\theta[\![(\mu/\mu_1)(-v' + v - u_\theta + \tfrac{1}{2}(u_\theta' + v''))]\!] + 2\delta_\theta^2[\![(\mu/\mu_1)(u' - u - v_\theta)]\!]$$
$$-2\delta_x\delta_\theta[\![(\mu/\mu_1)(v_x + w_\theta)]\!] + 2\delta_x^2[\![(\mu/\mu_1)(u' - w_x)]\!] + 2\delta\delta_x[\![(\mu/\mu_1)(u_x' + w'')]\!].$$

Appendix B. Derivation of the amplitude equations

We follow the methodology of Renardy (1989). The components of the adjoint eigenvector b_1 at (r, θ, x) are denoted by $h_1, \ldots, h_{18}$. These components correspond to the 18 components of the governing equations and conditions set out in Appendix A. The components of b_2 are (h_1, h_2, $-h_3$, h_4, h_5, h_6, $-h_7$, h_8, h_9, h_{10}, $-h_{11}$, h_{12}, h_{13}, $-h_{14}$, h_{15}, h_{16}, $-h_{17}$, h_{18}). The normalization condition is

$$(b_i, \mathrm{B}\zeta_i) = \delta_{ij}, \ i, j = 1, 2. \tag{B 1}$$

Here, b_1 and ζ_1 are $\sim \exp(\mathrm{i}\theta)$, $\zeta_2 \sim \exp(-\mathrm{i}\theta)$, so that $(\boldsymbol{b}_1, \mathrm{B}\zeta_2)$ is zero from the integral over θ.

Any real-valued function Φ can be decomposed in the form

$$\Phi = \Phi_1 + \Psi, \quad \Phi_1 = \sum_{i=1}^{2} z_i\zeta_i + \sum_{i=1}^{2} \bar{z}_i\bar{\zeta}_i, \tag{B 2}$$

where z_i are complex time-dependent amplitudes and Ψ represents a linear combination of eigenvectors (and possibly generalized eigenvectors) belonging to stable eigenvalues.

Suppose Ψ represents an eigenvector belonging to an eigenvalue s, not equal to $\omega_1(\lambda)$. Then $\mathrm{L}(s)\Psi = 0$ and hence $(b_i, (\mathrm{A}+s\mathrm{B})\Psi) = 0$. But $\mathrm{A}^* b_i = -\bar{\omega}_1(\lambda)\mathrm{B}^* b_i$ and thus $(b_i, (\mathrm{A} + s\mathrm{B})\Psi) = (b_i, \mathrm{A}\Psi) + s(b_i, \mathrm{B}\Psi) = (\mathrm{A}^* b_i, \Psi) + s(b_i, \mathrm{B}\Psi) = (-\omega_1(\lambda) + s)(b_i, \mathrm{B}\Psi)$. Therefore, $(b_i, \mathrm{B}\Psi) = 0$, $i = 1, 2$. Since $(b_i, (\mathrm{A} + \omega_1(\lambda)\mathrm{B})\Psi) = 0$, we also have $(b_i, \mathrm{A}\Psi) = 0$, $i = 1, 2$. We have $(\mathrm{A} + \bar{\omega}_1(\lambda)\mathrm{B})\bar{\zeta}_i = 0$, hence $(b_j, (\mathrm{A} + \bar{\omega}_1(\lambda)\mathrm{B})\bar{\zeta}_i) = 0$, and together with $\bar{\omega}_1 \neq \omega_1$, we conclude that $(b_j, B\bar{\zeta}_i) = 0$ for $i, j = 1, 2$.

We take the inner product of $\mathrm{B}\Phi$ with b_i, where Φ satisfies the expansion (B 2), and make use of the normalization (B 1), and obtain

$$z_i = (b_i, \mathrm{B}\Phi),\ i = 1, 2.$$

A projection operator Π is defined such that it picks out the components of Φ that consist of the critical modes and annihilates the stable modes: $\Pi\Phi = 2\,\mathrm{Re}(\sum_{i=1}^{2}(b_i, \mathrm{B}\Phi)\zeta_i)$, so that $\Psi = (I - \Pi)\Phi$ in the above decomposition. We can define an analogous decomposition of a function f which represents right-hand sides for the equations, i.e. components f_1 to f_{18}. This decomposition is motivated by the normalization condition (B 1) and the decomposition (B 2): $f = \sum_{i=1}^{2}(b_i, f)\mathrm{B}\zeta_i + \sum_{i=1}^{2}(\bar{b}_i, f)\mathrm{B}\bar{\zeta}_i + g$. Here $(b_i, g) = 0$, $i = 1, 2$. With the projection operator $\tilde{\Pi}$ defined as $\tilde{\Pi} f = 2\,\mathrm{Re}(\sum_{i=1}^{2}(b_i, f)\mathrm{B}\zeta_i)$, we have $g = (I - \tilde{\Pi})f$.

The inner product of (2.6) with b_i is formed, where $\mathrm{L}\Phi = (\mathrm{A} + \mathrm{B}\,\mathrm{d}/\mathrm{d}t)\Phi$. Using $(b_i, \mathrm{A}\Phi) = -\omega_1(\lambda)(b_i, \mathrm{B}\Phi)$, we obtain

$$\frac{\mathrm{d}z_i}{\mathrm{d}t} - \omega_1(\lambda)z_i = (b_i, \mathrm{N}_2(\Phi, \Phi) + \mathrm{N}_3(\Phi, \Phi, \Phi)),\ i = 1, 2. \tag{B 3}$$

Next, the projection $I - \tilde{\Pi}$ is applied to (B 2). Since $\mathrm{A}\zeta_i = -\omega_1(\lambda)\mathrm{B}\zeta_i$, $\mathrm{L}\Phi = \sum_{i=1}^{2}(\mathrm{d}/\mathrm{d}t - \omega_1)z_i\mathrm{B}\zeta_i + \sum_{i=1}^{2}(\mathrm{d}/\mathrm{d}t - \bar{\omega}_1)\bar{z}_i\mathrm{B}\bar{\zeta}_i + \mathrm{L}\Psi$. The application of $I - \tilde{\Pi}$ to the terms under summations yields zero. Hence $(I - \tilde{\Pi})\mathrm{L}\Phi = (I - \tilde{\Pi})\mathrm{L}\Psi$. Using $(b_i, \mathrm{B}\Psi) = 0$ and $(b_i, \mathrm{A}\Psi) = 0$, $\tilde{\Pi}\,\mathrm{L}\Psi = 0$ and thus

$$\left(\mathrm{A} + \mathrm{B}\frac{\mathrm{d}}{\mathrm{d}t}\right)\Psi = \mathrm{N}_2(\Phi, \Phi) + \mathrm{N}_3(\Phi, \Phi, \Phi) - 2\,\mathrm{Re}\left(\sum_{i=1}^{2}(b_i, \mathrm{N}_2(\Phi, \Phi) + \mathrm{N}_3(\Phi, \Phi, \Phi))\mathrm{B}\zeta_i\right). \tag{B 4}$$

Only quadratic terms in the asymptotic approximation to the centre manifold $\Psi = \tau(z_1, z_2)$ are required. Thus, for small solutions,

$$\Psi = \Psi_2 + \ldots, \qquad \Psi_2 = 2\,\mathrm{Re}\left(\sum_{i,j=1}^{2} z_i z_j \psi_{ij} + z_i \bar{z}_j \chi_{ij}\right),$$

where the dots indicate terms of order higher than quadratic. The small periodic solutions, taking into account the nonlinear terms, are found on the centre manifold. These are solutions close to the linear eigenfunctions.

Without loss of generality, the symmetry conditions $\psi_{ij} = \psi_{ji}$, $\chi_{ij} = \bar{\chi}_{ji}$, $i, j = 1, 2$, are assumed. The expansion for Ψ is inserted into (B 4) and (B 3) is used to express the time derivatives $\mathrm{d}z_i/\mathrm{d}t$. By comparing quadratic terms, we obtain

$$(\mathrm{A} + 2\omega_1(\lambda))\mathrm{B})\psi_{ij} = \mathrm{N}_2(\zeta_i, \zeta_j) - \sum_{k=1}^{2}(b_k, \mathrm{N}_2(\zeta_i, \zeta_j))\mathrm{B}\zeta_k - \sum_{k=1}^{2}(\bar{b}_k, \mathrm{N}_2(\zeta_i, \zeta_j))\mathrm{B}\bar{\zeta}_k,$$

$$\mathrm{A}\chi_{ij} = \mathrm{N}_2(\zeta_i, \bar{\zeta}_j) - \sum_{k=1}^{2}(b_k, \mathrm{N}_2(\zeta_i, \bar{\zeta}_j))\mathrm{B}\zeta_k - \sum_{k=1}^{2}(\bar{b}_k, \mathrm{N}_2(\zeta_i, \bar{\zeta}_j))\mathrm{B}\bar{\zeta}_k,$$

for $i, j = 1, 2$. In the computation of the ψ_{ij} and χ_{ij}, many of the inner products vanish. When the inner product of a vector with b_i is calculated, only those terms with the same x and θ dependences as the corresponding eigenfunction ζ_i remain and the rest are zero. For example, in the equation for ψ_{11}, $\mathrm{N}_2(\zeta_1, \zeta_1)$ is proportional to $\exp(2\mathrm{i}\alpha x + 2\mathrm{i}\theta)$ and none of the ζ_k or $\bar{\zeta}_k$ has this dependence, so the summation terms vanish. Moreover, we only need to evaluate ψ_{11} at $\lambda = 0$, and hence we

compute it from $(\mathrm{A}+2\omega_1(0)\mathrm{B})\psi_{11}=\mathrm{N}_2(\zeta_1,\zeta_1)$. Similarly, the summation terms in the χ_{ij} equations drop out altogether and we have $(\mathrm{A}+2\omega_1(0)\mathrm{B})\psi_{ij}=\mathrm{N}_2(\zeta_i,\zeta_j)$, $\mathrm{A}\chi_{ij}=\mathrm{N}_2(\zeta_i,\bar{\zeta}_j)$, where $i,j=1,2$, and $\omega_1(0)=\mathrm{i}\omega$.

The equations governing the components (u,v,w,p,δ) for χ_{11} decouple and we discuss them here. Since χ_{11} has no Fourier dependence on x and θ, incompressibility implies $ru'+u=0$, which together with the boundary condition yields $u=0$ in the entire domain. Putting $\mathrm{d}/\mathrm{d}x$ and $\mathrm{d}/\mathrm{d}\theta$, the equations for the variables decouple. The pressure p in χ_{11} satisfies

$$r^2p'=H_2 \text{ of } \mathrm{N}_2(\zeta_1,\bar{\zeta}_1), \qquad (1/\zeta)r^2p'=H_6 \text{ of } \mathrm{N}_2(\zeta_1,\bar{\zeta}_1),$$

$$-\mathbb{R}_1[\![p]\!]-\frac{J}{\mathbb{R}_1}\delta=H_{15} \text{ of } \mathrm{N}_2(\zeta_1,\bar{\zeta}_1).$$

Since there is a family of modes $p=$constant, $u=v=w=\delta=0$, we eliminate them by requiring that $p_1=0$ at $r=1$. The component v of χ_{11} satisfies

$$-(1/\mathbb{R}_1)(-v+rv'+r^2v'')=H_3 \text{ of } \mathrm{N}_2(\zeta_1,\bar{\zeta}_1),\ -(1/\mathbb{R}_2)(-v+rv'+r^2v'')=H_7 \text{ of } \mathrm{N}_2(\zeta_1,\bar{\zeta}_1),$$

$$v_1-v_2=H_{11} \text{ of } \mathrm{N}_2(\zeta_1,\bar{\zeta}_1), \qquad [\![(\mu/\mu_1)(v'-v)]\!]=H_{14} \text{ of } \mathrm{N}_2(\zeta_1,\bar{\zeta}_1),$$

and the boundary condition is $v=0$ at $r=a$. The component w of χ_{11} satisfies

$$-(1/\mathbb{R}_1)(rw'+r^2w'')=H_4 \text{ of } \mathrm{N}_2(\zeta_1,\bar{\zeta}_1),$$

$$-(1/\mathbb{R}_2)(rw'+r^2w'')=H_8 \text{ of } \mathrm{N}_2(\zeta_1,\bar{\zeta}_1),$$

$$w_1-w_2+\delta[\![W']\!]=H_{12} \text{ of } \mathrm{N}_2(\zeta_1,\bar{\zeta}_1), \quad [\![(\mu/\mu_1)w']\!]+\delta[\![(\mu/\mu_1)W'']\!]=H_{13} \text{ of } \mathrm{N}_2(\zeta_1,\bar{\zeta}_1),$$

and the boundary condition is $w=0$ at $r=a$. The H_9,H_{10} of $\mathrm{N}_2(\zeta_1,\bar{\zeta}_1)$ are 0. Also, for this zeroth Fourier component, we need to evaluate δ in order to conserve volume. This yields, for the core radius at $r=1+h(x,\theta)$,

$$\int_{\theta=0}^{2\pi}\int_{x=0}^{2\pi/\alpha_c}(1+h)^2\mathrm{d}\theta\mathrm{d}x=\int\int 1\mathrm{d}\theta\mathrm{d}x, \ \rightarrow \ \int\int 2h+h^2\mathrm{d}\theta\mathrm{d}x=0. \tag{B 5}$$

The Fourier expansion of the interface perturbation is

$$h=\sum_{n=-\infty}^{\infty}\sum_{m=-\infty}^{\infty}h_{mn}\mathrm{e}^{\mathrm{i}n\theta+\mathrm{i}m\alpha_c x},$$

corresponding to the expansion for the solution (B 2) where, for example, h_{11} is the interface perturbation (δ) from the mode ζ_1 and h_{-1-1} is the interface perturbation (δ) from the mode $\bar{\zeta}_1$. Equation (B 5) correct to quadratics yields $2h_{00}+2h_{11}h_{-1-1}=0$. Here, h_{00} is composed of the interface perturbation δ for χ_{11} and for $\bar{\chi}_{11}$. Thus the δ for χ_{11} is $-\frac{1}{2}(\delta \text{ of } \zeta_1)(\delta \text{ of } \bar{\zeta}_1)$. We use this in the equations above. The pressure gradient in the axial direction in the nonlinear analysis is fixed, since we are not introducing a perturbational $\mathrm{d}p/\mathrm{d}x$.

We obtain from (B 3)

$$\frac{\mathrm{d}z_i}{\mathrm{d}t}-\omega_1(\lambda)z_i=(b_i,\mathrm{N}_2(\Phi_1,\Phi_1))+(b_i,\mathrm{N}_3(\Phi_1,\Phi_1,\Phi_1))+2(b_i,\mathrm{N}_2(\Phi_1,\Psi_2)), \quad i=1,2. \tag{B 6}$$

The quadratic term $\mathrm{N}_2(\Phi_1,\Phi_1)$ contains all combinations of the interactions of the eigenfunctions, and there are no terms with the same x and θ dependences as the

vectors ζ_i: thus, the first inner product vanishes. This system is of the form

$$\frac{\mathrm{d}z_i}{\mathrm{d}t} = F_i(z_1, z_2, \lambda), \quad i = 1, 2. \tag{B 7}$$

There is further simplification because some of the coefficients in (B 6)–(B 7) are related to each other. The symmetry under reflection $n \to -n, v \to -v$ changes ζ_1 to ζ_2, b_1 to b_2, ψ_{11} to ψ_{22}, ψ_{12} stays as it is, χ_{11} to χ_{22}, χ_{12} to χ_{21}, F_1 to F_2, and so on. Hence, $(b_2, \mathrm{N}_2(\chi_{22}, \zeta_2)) = (b_1, \mathrm{N}_2(\chi_{11}, \zeta_1))$, $(b_2, \mathrm{N}_2(\psi_{22}, \bar{\zeta}_2)) = (b_1, \mathrm{N}_2(\psi_{11}, \bar{\zeta}_1))$. In this way, we can relate the coefficients in F_2 to the coefficients in F_1. This leaves two coefficients in the normal form equations:

$$\left.\begin{aligned} F_1(z_1, z_2, \lambda) &= \omega_1(\lambda) z_1 + \beta_1(\lambda)|z_1|^2 z_1 + \beta_2(\lambda)|z_2|^2 z_1, \\ F_2(z_1, z_2, \lambda) &= \omega_1(\lambda) z_2 + \beta_1(\lambda)|z_2|^2 z_2 + \beta_2(\lambda)|z_1|^2 z_2; \end{aligned}\right\} \tag{B 8}$$

$$\left.\begin{aligned} \beta_1(\lambda) &= (b_1, 2\mathrm{N}_2(\bar{\zeta}_1, \psi_{11}) + 4\mathrm{N}_2(\zeta_1, \chi_{11}) + 3\mathrm{N}_3(\zeta_1, \zeta_1, \bar{\zeta}_1)), \\ \beta_2(\lambda) &= (b_1, 4\mathrm{N}_2(\bar{\zeta}_2, \psi_{12}) + 4\mathrm{N}_2(\zeta_2, \chi_{12}) + 4\mathrm{N}_2(\zeta_1, \chi_{22}) + 6N_3(\zeta_1, \zeta_2, \bar{\zeta}_2)). \end{aligned}\right\} \tag{B 9}$$

We let $\omega_1(\lambda) = \mathrm{i}\omega + \epsilon_1$, where ω and the bifurcation parameter ϵ_1 are real.

REFERENCES

Bai, R., Chen, K. & Joseph, D. D. 1992 Lubricated pipelining: stability of core–annular flow. Part 5. Experiments and comparison with theory. *J. Fluid Mech.* **240**, 97–132.

Boomkamp, P. A. M. & Miesen, R. H. M. 1992 Nonaxisymmetric waves in core–annular flow with a small viscosity ratio. *Phys. Fluids* A **4**, 1627–1636.

Chandrasekhar, S. 1961 *Hydrodynamic and Hydromagnetic Stability*. Oxford University Press.

Fujimura, K. & Renardy, Y. Y. 1995 The 2:1 steady/Hopf mode interaction in the two-layer Benard problem. *Physica* D **85**, 25–65.

Gottlieb, D. & Orszag, S. A. 1977 *Numerical Analysis of Spectral Methods: Theory and Applications.* SIAM.

Hu, H. H. & Patankar, N. 1995 Non-axisymmetric instability of core–annular flow. *J. Fluid Mech.* **290**, 213–224.

Joseph, D. D., Bai, R., Chen, K. & Renardy, Y. 1997 Core–annular flows. *Ann. Rev. Fluid Mech.* **29**.

Joseph, D. D. & Renardy, Y. Y. 1993 *Fundamentals of Two-Fluid Dynamics, Part 1: Mathematical Theory and Applications, Part 2: Lubricated Transport, Drops and Miscible Liquids.* Springer.

Joseph, D. D., Renardy, Y. & Renardy, M. 1983 Instability of the flow of immiscible liquids with different viscosities in a pipe *J. Fluid Mech.* **141**, 309–317. (Longer version available as University of Wisconsin-Madison Mathematics Research Center Report).

Orszag, S. A. 1971 Accurate solution of the Orr-Sommerfeld stability equation. *J. Fluid Mech.* **50**, 689–703.

Preziosi, L., Chen, K. & Joseph, D. D. 1989 Lubricated pipelining: stability of core–annular flow. *J. Fluid Mech.* **201**, 323–356.

Renardy, M. & Renardy, Y. 1993 Derivation of amplitude equations and analysis of sideband instabilities in two-layer flows. *Phys. Fluids* A **5**, 2738–2762.

Renardy, Y. 1989 Weakly nonlinear behavior of periodic disturbances in two-layer Couette–Poiseuille flow. *Phys. Fluids* A **1**, 1666–1676.

Ruelle, D. 1973 Bifurcations in the presence of a symmetry group. *Arch. Rat. Mech. Anal.* **51**, 136.